Nanoscale

ROYAL SOCIETY OF CHEMISTRY

PAPER

View Article Online
View Journal | View Issue

Cite this: *Nanoscale*, 2020, **12**, 9786

DNA-directed arrangement of soft synthetic compartments and their behavior *in vitro* and *in vivo*†

Juan Liu,‡§[a] Ioana Craciun,‡[a] Andrea Belluati,[a] Dalin Wu,[a] Sandro Sieber,[b] Tomaz Einfalt,[b] Dominik Witzigmann,¶[b] Mohamed Chami,[c] Jörg Huwyler[b] and Cornelia G. Palivan *[a]

DNA has been widely used as a key tether to promote self-organization of super-assemblies with emergent properties. However, control of this process is still challenging for compartment assemblies and to date the resulting assemblies have unstable membranes precluding *in vitro* and *in vivo* testing. Here we present our approach to overcome these limitations, by manipulating molecular factors such as compartment membrane composition and DNA surface density, thereby controlling the size and stability of the resulting DNA-linked compartment clusters. The soft, flexible character of the polymer membrane and low number of ssDNA remaining exposed after cluster formation determine the interaction of these clusters with the cell surface. These clusters exhibit *in vivo* stability and lack of toxicity in a zebrafish model. To display the breadth of therapeutic applications attainable with our system, we encapsulated the medically established enzyme laccase within the inner compartment and demonstrated its activity within the clustered compartments. Most importantly, these clusters can interact selectively with different cell lines, opening a new strategy to modify and expand cellular functions by attaching such pre-organized soft DNA-mediated compartment clusters on cell surfaces for cell engineering or therapeutic applications.

Received 13th January 2020,
Accepted 19th April 2020

DOI: 10.1039/d0nr00361a

rsc.li/nanoscale

1. Introduction

The unique features of DNA enable the organization of nanostructures into larger superstructures and macroscopic superlattices with well-defined orientations depending on their intrinsic architecture.[1,2] Current knowledge and experiences with DNA-organized supramolecular structures revolve around exploiting DNA-linked rigid nanostructures,[3,4] for example gold nanoparticles.[5,6] The rigidity of particles imparts directionality to hybridization interactions and the high-density of DNA strands on the surfaces act as 'valencies' to manipulate the stereo-organization precisely, either when DNA chains or DNA origami direct the organization,[7–9] or when steric hindrance induces formation of core-satellite structures.[5,7,10,11]

A completely different framework of interactions is induced when the nanostructure is deformable, and molecules can laterally diffuse inside the assembly, causing a constant fluctuation in exposed molecular groups bearing the DNA. Thus, the unique properties of the resulting organization open up a new field of soft DNA-linked compartment assemblies. Only recently have soft nanocompartments, especially liposomes and polymersomes, been exploited for DNA-mediated organization[12,13] due to the preconception that their inherent flexibility interferes with the creation of defined structures,[14] such as superlattices assembled by rigid nanoparticles. For example, in the case of liposomes, DNA-mediated assembly led to their precipitation from solution or membrane fusion due to their low stability.[13,15,16] In the case of polymersome based sub-micrometer sized assemblies, only one example has been reported[12] with no *in vitro* or *in vivo* testing, thus insights into the behavior of such soft materials in a biological environment are still lacking. Nevertheless, nanocompartments have unique advantages due to their intrinsic architecture, hollow spheres with hydrophilic cavities surrounded by a membra-

[a]*Department of Chemistry, University of Basel, Mattenstrasse 24a, Basel-4058, Switzerland. E-mail: cornelia.palivan@unibas.ch*
[b]*Division of Pharmaceutical Technology, Department of Pharmaceutical Sciences, University of Basel, Klingelbergstrasse 50, Basel-4056, Switzerland*
[c]*BioEM lab, Biozentrum, University of Basel, Mattenstrasse 26, Basel-4058, Switzerland*

†Electronic supplementary information (ESI) available. See DOI: 10.1039/d0nr00361a

‡These authors contributed equally to this work.

§Present address: Chemistry Research Laboratory, Department of Chemistry, University of Oxford, 12 Mansfield Road, OX1 3TA, Oxford, UK.
¶Present address: Department of Biochemistry and Molecular Biology, University of British Columbia, 2350 Health Sciences Mall, Vancouver, British Columbia-V6T 1Z3, Canada.

nous structure possessing hydrophobic cores. They enable the efficient loading of various hydrophilic and hydrophobic therapeutic agents ranging from small molecular weight drugs to DNA and RNA for drug delivery,[17–21] nanoparticles for catalytic properties,[22,23] and various enzymes for the development of artificial organelles[24] functional *in vivo*.[25] While both liposomes and polymersomes allow tailoring for biocompatibility, stimuli-responsiveness and biodegradability, polymersomes are an improved alternative as they exhibit higher mechanical stability compared to their counterpart, liposomes.[24,26–28]

There are several examples of sub-micrometer sized nanoparticle assemblies, however, only a few were proposed for cellular interactions and phototherapies.[5,10,29,30] The biological application of such nanoparticle assemblies remains challenging with most focusing on DNA intercalating molecules loaded non-covalently in the hybridized DNA strands for their delivery.[5,30,31] Furthermore such nanoparticle assemblies undergo fast disassembly *in vitro* and *in vivo*,[10,30] implemented as a strategy for clearance.[10]

Here, we present soft DNA-linked polymersome clusters as a new type of compartment-assembly able to support efficient bio-applications with the unique advantage of simultaneously allowing the encapsulation of catalytic compounds and their localization at desired locations controlled by their interaction with cells. DNA-linked polymersomes represent a complementary platform to DNA–nanoparticle systems with a hierarchic self-organization that has been manipulated by fine-tuning the polymer membrane composition, the surface density of ssDNA and polymersome concentration (Scheme 1). As the soft polymersome clusters differ greatly with respect to other DNA-mediated assemblies, we methodically probe their behavior *in vitro* and *in vivo* to determine their suitability for future applications. We present how such soft DNA-mediated compartment assemblies interact with different cell lines resulting in binding selectivity towards epithelial cells *via* scavenger receptors. Notably, for the first time the realization of cellular membrane attachment of DNA-linked super-assemblies is achieved. These clusters are non-toxic and their characteristic behavior is also maintained *in vivo*. Attachment of such clusters to the cell surface could prove momentous, as it would provide a universal and innocuous approach for non-genetic therapeutic cell engineering[32,33] but also detoxification of xenotoxins by encapsulating enzymes within the inner compartment. Following along this line, we encapsulated laccase as an extensively studied enzyme with multiple applications[34,35] within the clustered polymersomes and demonstrated the catalytic potential of the clusters to prevent internalization of harmful compounds inducing apoptosis. In contrast to rigid DNA-linked nanoparticles and assemblies that offer limited bioactivity after endocytosis, we reveal that both the deformability of the polymersome's membrane and the lateral diffusion of the polymer chains within the membrane contribute to their surprising stability and determine the clusters' destiny in biologically relevant environments. The multiple compartments with both aqueous cavities and hydrophobic boundaries benefit the integration of active biomolecules with diverse chemical properties into one nanoplatform, providing combined and synchronized therapeutic and diagnostic solutions. All these features make them truly unique soft compartment assemblies with high potential for bio-applications, such as regenerative medicine or cell engineering to restore, replace or integrate new cellular functions.

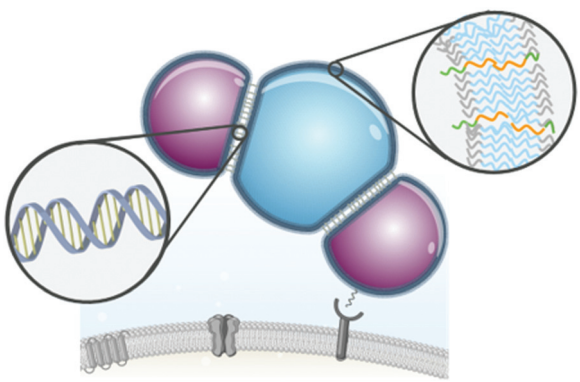

Scheme 1 Synthetic nanocompartments (polymersomes, shown in blue and magenta) assembled from amphiphilic diblock copolymers (right insert depicting the polymeric membrane) are interconnected using DNA hybridization as the driving force for their self-organization into clusters (left insert highlighting the hybridized DNA that locks in place the polymersomes). Such soft flexible assemblies selectively interact with the scavenger receptors on the cell membranes *in vitro* and *in vivo* leading to attachment to the cell surface.

2. Results and discussion

2.1. Assembly of ssDNA functionalized polymersomes and DNA-linked polymersome clusters

In order to construct stable sub-micrometer sized polymersome clusters in a controllable manner, we carefully considered three key molecular factors: (i) the chemical nature and morphology of the polymersomes' membrane, (ii) the DNA density and distribution on the polymersomes' surface, and (iii) the concentration of polymersomes.[12] For polymersome formation, we selected the diblock copolymer poly(dimethylsiloxane)-*block*-poly(2-methyloxazoline) (PDMS-PMOXA) because of its low toxicity and biocompatibility.[36,37] As previously shown, the combination of PMOXA-PDMS-PMOXA triblock copolymer with azide-functionalized diblock PDMS-PMOXA copolymer, bearing a longer PMOXA block, forms polymersomes with exposed azide functional groups on the polymersomes' surface.[12] We then linked dibenzocyclooctyne (DBCO)-functionalized ssDNA (DBCO-ssDNA) to the polymersomes and promoted their zipping by DNA hybridization.[12] Here we changed the approach and synthesized only diblock copolymers, $PDMS_{62}$-$PMOXA_{13}$ and $PDMS_{71}$-$PMOXA_{25}$-OEG_3-N_3, with similar PDMS block lengths aimed at circumventing hydrophobic mismatch and phase separation between the two polymers, consequently favoring formation of polymersomes (Fig. 1A, Fig. S1, and Table S1†). Switching to this new

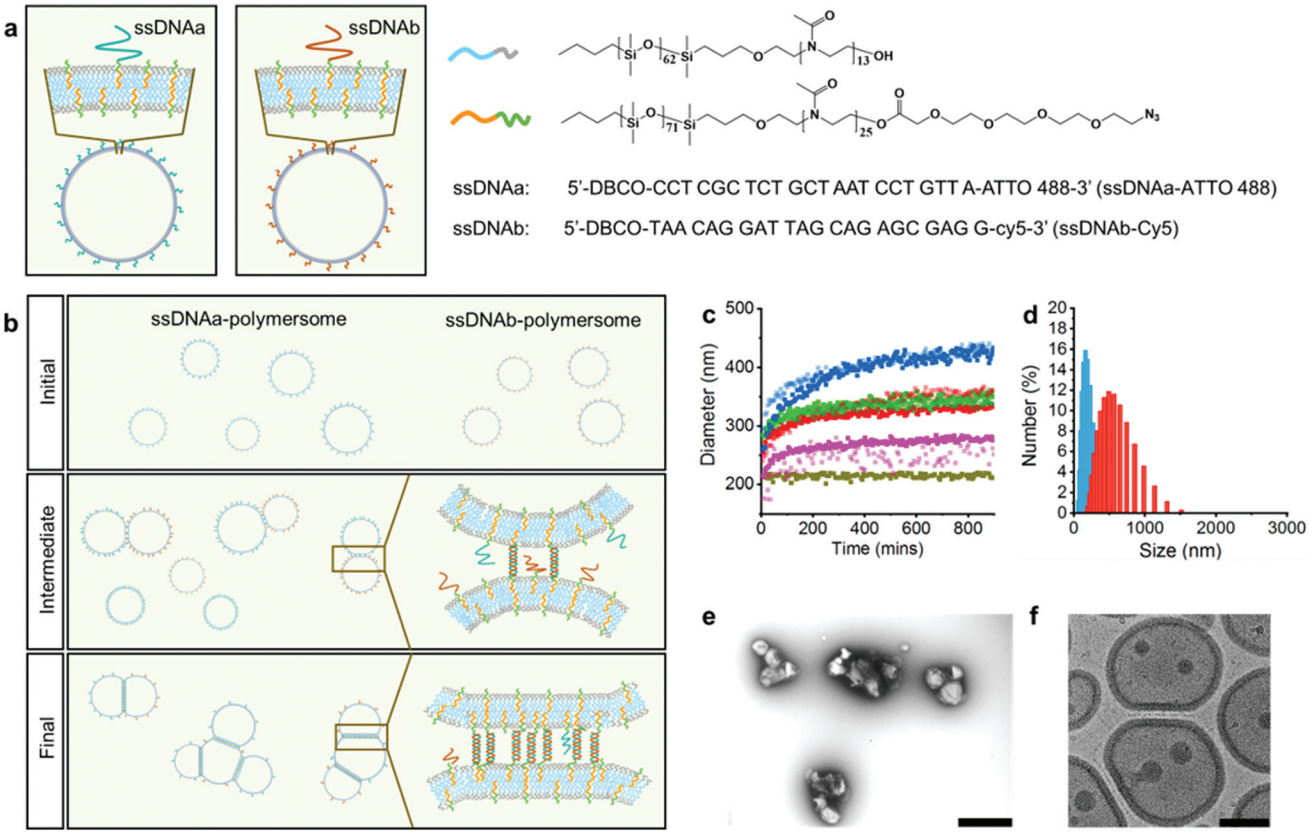

Fig. 1 Principles and preparation of DNA-linked polymersome clusters. (A) Schematic representation of assembled ssDNA–polymersomes, chemical structures of the two block copolymers used and the sequence of the two complementary ssDNAs. (B) Schematic representation of the cluster assembly process where the polymersomes first link together *via* DNA hybridization, followed by migration of non-hybridized ssDNAs and subsequent hybridization to form a DNA bridge area in between the polymersomes. (C) Self-organization of ssDNA–polymersomes into clusters reported as the change in their apparent D_H as a function of time for 0.5 mol% (orange and light orange), 1 mol% (magenta and light magenta), 5 mol% (red and light red), 10 mol% (green and light green) and 20 mol% (blue and light blue) azide-functionalized diblock copolymers. The results represent two independent measurements shown on the graph as hues of the same color. (D) The distribution of the average apparent D_H of: ssDNAa-polymersomes (200 nm ± 30 nm, s.e.m, n = 3,) comprised of 20 mol% azide-functionalized diblock copolymers (blue) and of the corresponding DNA-linked polymersome clusters (440 nm ± 100 nm, s.e.m, n = 3) (red). (E–F) Transmission electron microscopy (TEM) and cryo-TEM micrographs of the DNA-linked polymersome clusters P20-ab. Scale bars are 500 nm (E) and 100 nm (F).

block copolymer combination facilitated an increase in $PDMS_{71}$-$PMOXA_{25}$-OEG_3-N_3 content to 20 mol% without perturbing the self-assembly (Fig. S2†), thus obtaining polymersomes with average apparent hydrodynamic diameter (D_H) of 190 ± 30 nm (s.e.m, n = 3) as obtained by dynamic light scattering (DLS, Fig. S4 and Table S2†).

As mentioned above, key molecular factors that affect the process of hierarchic self-organization of polymersomes into clusters are both the number of ssDNAs per polymersome and concentration of ssDNA–polymersomes. To modulate the apparent D_H of DNA-linked polymersome clusters, we kept the concentration of complementary ssDNA–polymersomes constant (0.2 mg mL^{-1}) and varied only the number of ssDNAs per polymersome. We linked DBCO-ssDNAs onto the polymersomes' surface by strain-promoted azide–alkyne cycloaddition (SPAAC) reaction between DBCO-ssDNAs and polymersomes with exposed N_3 groups. By varying the N_3 content per polymersome, we varied the number of ssDNAs per polymersome from 1 ± 1 to 289 ± 72, as measured by fluorescence correlation spectroscopy (FCS, Fig. S3, see ESI† for details). The perikinetic clustering (solely driven by diffusion) of complementary ssDNA–polymersomes, at equal mass ratios and 37 °C, was investigated by monitoring the change in apparent D_H over time (Fig. 1B and C). The hybridization of complementary ssDNA on the polymersome surface resulted in a rapid increase in the apparent D_H until reaching a plateau with a defined range, where controlled cluster formation occurs. Self-organization into sub-micrometer sized clusters takes place only for complementary ssDNA–polymersomes with a number of linked ssDNAa/b ranging from 34 ± 33 to 188 ± 58 and 8 ± 5 to 111 ± 29 (Fig. S3 and S4†), corresponding to 1 to 20 mol% of azide-functionalized diblock content, respectively (Fig. 1E and F). Lowering the amount of linked ssDNA per polymersome does not sustain cluster formation, while a higher number of ssDNA per polymersome resulted in uncontrollable aggregation, as observed by the instantaneous formation of large clusters with an apparent D_H > 1 μm.

Ultimately, we obtained a series of polymersome clusters with a size distribution corresponding to a lognormal distribution function (statistical analysis, ESI†) and an average apparent D_H from 280 ± 80 nm to 440 ± 100 nm (s.e.m., n = 3, Fig. 1D and Fig. S4†). The distribution of the number of polymersomes/cluster for polymersomes with 1 to 20 mol% azide-functionalized diblock content was fitted with a log-normal distribution function as well (statistical analysis, ESI†). The clusters are composed on average of 2.5 ± 1.3 to 3.4 ± 1.6 polymersomes per cluster with a non-bound polymersome fraction lower than 5%, determined from transmission electron microscopy (TEM, Fig. S4†). In contrast with ssDNA-coupled rigid nanoparticles, ssDNA–polymersomes are advantageous when forming sub-micrometer sized clusters in a controllable manner as the ssDNA-bearing block copolymers migrate through the membrane and are then locked in a bridging area between linked polymersomes (Fig. 1B and F).[12,38] The formation of this three-dimensional bridging area with an area regulated by the number of dsDNAs holding the polymersomes together and opening dependent on the length of dsDNA, rather than a 'spot', functions as a barrier thus sheltering the dsDNA from exposure to the environment. The migration of ssDNA to the bridging area also decreases the ssDNA density in the non-bridging area and eventually terminates the clustering process. Therefore, the formation of sub-micrometer sized clusters is kinetically controlled by using mechanically stable polymersomes with a relatively low ssDNA density on the surface to prevent aggregation or rupture.

To further probe the stability of the bridging region, we incubated the clusters in presence of DNase I, the most prevalent endonuclease in serum (Fig. S5†). We observed that polymersome clusters with an apparent D_H above 300 nm remain clustered in presence of 1 μg mL^{-1} of DNase I. However, no clusters were formed when the ssDNA–polymersomes were pre-treated with 1 μg mL^{-1} of DNase I, suggesting the DNA strands on single ssDNA–polymersomes have been digested. Narrowing the bridging area between polymersomes from 7.1 ± 0.5 nm to 3.5 ± 0.3 nm by reducing the length of the ssDNA from 22 bp to 11 bp effectively protects the polymersome clusters against DNase I hydrolysis (Fig. S5†). The clusters linked by 22 bp DNA disassembled to single polymersomes at a DNase I concentration of 10 μg mL^{-1}, while clusters linked by 11 bp DNA preserved their clustered structures.

2.2. Examination of DNA-linked polymersome clusters' behavior *in vitro*

As the polymersome clusters we designed differ greatly with respect to other DNA-mediated assemblies, and no other soft compartment assemblies were studied *in vitro*, it was fundamental to study their interactions *in vitro* and determine their potential for biomedical applications. Under physiological conditions, *e.g.* in cell medium, the colloidal stability of DNA functionalized materials might be affected due to interactions between proteins and the DNA.[39] Thus, we first examined the stability of the 22 bp ssDNA–polymersome clusters in cell medium (Fig. S6A†). The clusters remained stable up to 10 hours due to the strong interactions between complementary ssDNAs located in the sheltered bridging region (Fig. S6A†).

Prior to determining if there are selective interactions between the clusters and epithelial cells, we evaluated the toxicity of the ssDNA polymersomes and DNA-linked clusters using an MTS assay (Fig. S6E†). No toxicity was obtained up to 40 μg mL^{-1}. Subsequently, we examined their interactions with three cell lines, *i.e.* HeLa, HEK293T and U87-MG, to determine if the DNA-linked polymersome clusters are stable, internalized or have any inherent selectivity towards a specific cell line. We incubated cells in the presence of low concentrations (13 μg mL^{-1}) of unmodified polymersomes, ssDNA–polymersomes, 400 nm sized small clusters and 1000 nm large clusters (see Methods for the preparation of large clusters). In polymersomes functionalized with 22 bp ssDNAa we encapsulated a fluorescent dye DY-633 (DY-633-P20-a) and in polymersomes functionalized with the complementary 22 bp ssDNAb ATTO 488 dye (ATTO-488-P20-b) as small molecule mimics and for visualization *via* confocal laser scanning microscopy (CLSM, Fig. S6C and D†). After 24 h, we thoroughly washed the cells to remove unbound polymersomes or clusters and stained the cellular membrane using the CellMask™ orange plasma membrane stain, prior to imaging. DY-633-P20-a as well as both small and large polymersome clusters accumulated on the cell surface predominantly at cell junctions of HEK293T and HeLa cells (Fig. 2A, Fig. S7A–C† for transmission channels, Fig. S8A–J and S9A–C† for repeat experiments). Using flow cytometry, we confirmed the presence of clusters, most likely still attached to the cell surface; however, the precise location cannot be determined using this technique (Fig. S10A and B†). Unmodified polymersomes showed no binding and were not internalized (Fig. S8B and G†). Furthermore, the binding interaction between the clusters with the cell membrane appears to be more favorable than the one between single ssDNA–polymersomes and cells, since rigorous washing steps prior to imaging did not result in detachment and there appear to be more clusters than single ssDNA–polymersomes retained on the cell membrane as shown by the fluorescence intensity (Fig. 2). A local accumulation of clusters on the cell surface is key feature that will allow their future application for biomedical applications. In addition, polymersome clusters have the advantages, opposed to non-clustered or ssDNA–polymersomes to provide segregated spaces at the nanoscale supporting simultaneous functionality of separate compounds and simultaneous co-localization of such comportments to improve their overall efficiency. As observed in the merged image, DY-633-P20-a overlaps with ATTO-488-P20-b, to a larger extent as compared to the control polymersomes bearing non-complementary ssDNA (Fig. 2B), indicating that the clusters are intact and did not dissociate over the 24 h incubation period. The large 1000 nm clusters appear to form a network like structure that expands to cover large portions of the cell outer membrane (Fig. 2C) suggesting an active rearrangement of the clusters *in vitro*. Binding and accumulation of the clusters to the cell surface occurred within the first hour of incu-

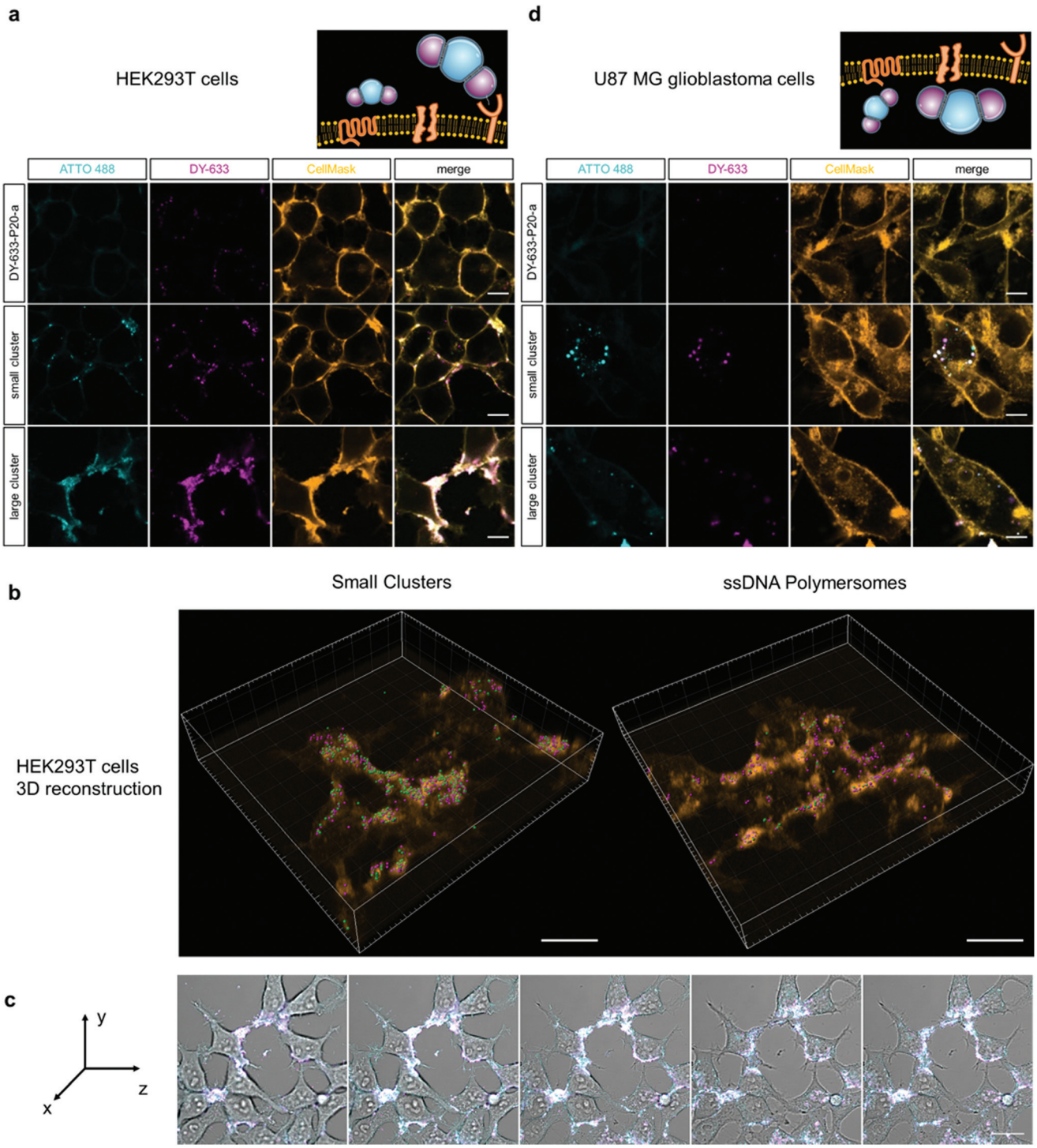

Fig. 2 Interaction of DNA-linked polymersome clusters with HEK293T and U87-MG cells. (A) CLSM micrographs showing attachment to surface of HEK293T cells of ssDNA polymersomes loaded with DY-633 (DY-633-P20-a, magenta), 400 nm small clusters and 1000 nm large clusters composed of ssDNAa-polymersomes loaded with DY-633 (DY-633-P20-a magenta) and ssDNAb-polymersomes loaded with ATTO 488 (ATTO-488-P20-b, cyan). Scale bar = 10 μm. (B) 3D *z*-stack reconstruction showing 400 nm clusters on the cell surface (left) and non-complementary ssDNA–polymersomes (right). Scale bar = 20 μm. (C) *Z*-Stack of large polymersome clusters forming a network on the surface of HEK293T cells. Scale bar = 20 μm. (D) CLSM micrographs showing uptake in U87-MG cells of ssDNA polymersomes loaded with DY-633 (DY-633-P20-a, magenta), 400 nm small clusters and 1000 nm large clusters composed of ssDNAa-polymersomes loaded with DY-633 (DY-633-P20-a, magenta) and ssDNAb-polymersomes loaded with ATTO 488 (ATTO-488-P20-b, cyan). Scale bar = 10 μm. The experiments were performed in cell media containing 10% fetal calf serum. The cell membrane was stained using CellMaskTM orange plasma membrane stain prior to imaging.

bation with no precipitation or accumulation visible in regions where the cells were not present, thus further demonstrating the high affinity of the clusters towards the cell surface (Fig. S11†). Binding to the cell surface is unique as most reported DNA coupled nanostructures and assemblies are internalized within cells and do not form networks on the surface.[5,10,29,30] This behavior is again an exceptional emerging property of using soft DNA-linked polymersomes bearing a low DNA surface density. This leads to a low adhesion energy for full wrapping of cells through receptor binding and thus might not be sufficient to activate endocytosis.[40] A second factor contributing to this unique behavior is that ssDNA–polymersomes and the DNA-linked polymersome clusters are much larger and more deformable compared to rigid gold nanoparticles where the stiffness of the surface promotes cell membrane engulfment.[41] In stark contrast, our clusters spread along the cell membrane without significant membrane deformation, thereby limiting the internalization processes.

Next, we examined the interaction of unmodified polymersomes, ssDNA–polymersomes and the small and large clusters with U87-MG glioblastoma cells, known to have a higher endocytotic potential and favor uptake of larger sized particles.[42,43] Interestingly, we observed limited internalization of both the 400 nm clusters and to a lesser extent of the larger clusters (Fig. 2D, Fig. S7D–F, S8K–P and S9D–E†). DY-633-P20-a and ATTO-488-P20-b polymersomes from within the cluster colocalize, as seen also from the individual CLSM *z*-stack slices (Fig. S8P†) indicating that the clusters preserve their integrity following uptake, as re-clustering within the cell is improbable (Fig. 2D). In the case of ssDNA–polymersomes and unmodified polymersomes it was difficult to determine the extent of uptake or attachment by CLSM due to their scarcity; however, analysis of the flow cytometry data suggests that both were internalized or in the case of ssDNA possibly attached to the cell surface (Fig. S10C†). As mentioned above, the precise location cannot be determined *via* flow cytometry, however unmodified polymersomes cannot attach to the cell surface and have been shown to be readily uptaken by cells.[25,44] The observed uptake *via* CLSM of the small and large clusters is in agreement with the fact that U87-MG cell line preferentially uptakes larger particles (Fig. S10C†).[42,43]

2.3. Mechanism of DNA-linked polymersome cluster attachment to cells

To better understand the *in vitro* behavior and specific cellular interaction of the polymersome clusters, we explored the binding mechanism of the ssDNA–polymersomes and clusters with HEK293T cells, as model cell line. Patel *et al.* showed that DNA-functionalized nanoparticles are internalized *via* binding to scavenger receptors.[45] To test whether our DNA-polymersome clusters also bind to this class of receptors, we performed competitive inhibition experiments. We preincubated the cells with increasing concentrations of two scavenger receptor ligands (*i.e.* polyinosinic acid (PolyI) and Fucoidan) for 1 hour prior to addition of ssDNA–polymersomes, small (400 nm) and large (1000 nm) clusters. As the concentration of the inhibitors increases, surface binding of the ssDNA–polymersomes, both small and large clusters, decreased in a dose responsive fashion as compared to controls (Fig. 3A, B depicting trend of large clusters and Fig. S12† transmission channel, Fig. S13† for complete analysis). At the highest concentration of PolyI, binding of the clusters was almost fully inhibited and

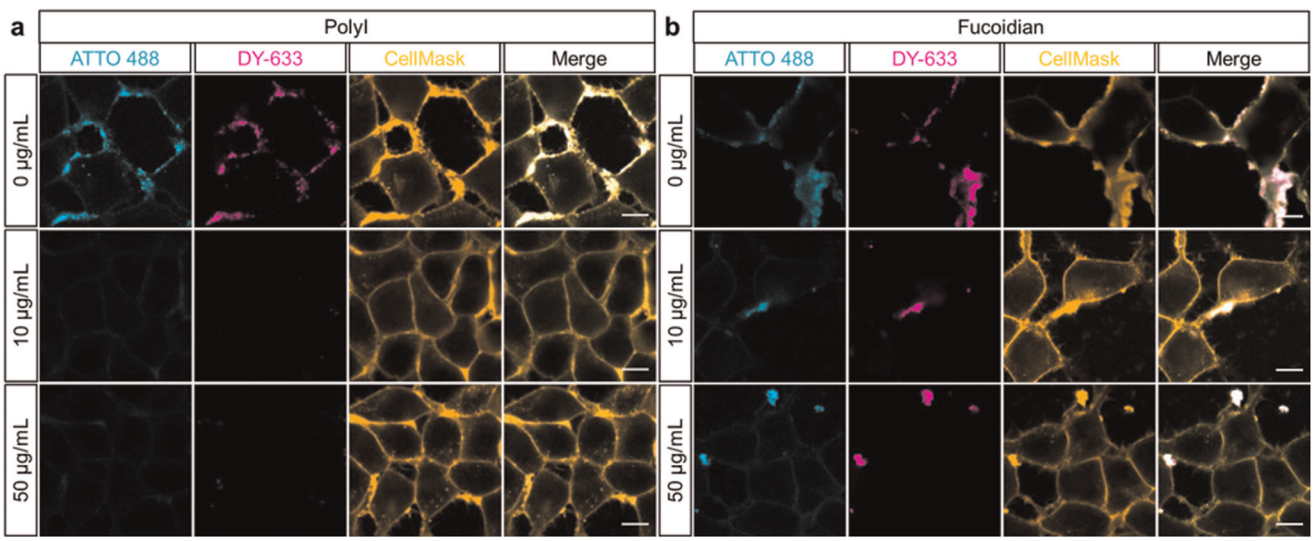

Fig. 3 Effect of scavenger receptor inhibitors on cluster cellular interaction. (A) CLSM micrographs of 1000 nm large DNA-linked polymersome clusters composed of ssDNAa-polymersomes loaded with DY-633 (DY-633-P20a, magenta) and ssDNAb-polymersomes loaded with ATTO-488 (ATTO-488-P20b, cyan) in presence of increasing concentration of PolyI, a scavenger receptor inhibitor (0 to 50 μg mL^{-1}, final concentration). Addition of PolyI completely inhibits cell binding of the DNA-linked polymersome clusters even at the lowest concentration tested. (B) CLSM micrographs of the 1000 nm large DNA-linked polymersome clusters in presence of increasing concentration of Fucoidan, a scavenger receptor inhibitor (0 to 50 μg mL^{-1}, final concentration). Scale bar 10 μm.

to a lesser extent in the case of the Fucoidan inhibitor. These results indicate that specific binding to epithelial cells is indeed mediated through attachment of negatively charged polymersome clusters to scavenger receptors. Of note, although DNA migration occurs during the polymersome clustering, approximately 50% of ssDNA on the polymersomes' surface remains non-hybridized. The percentage of non-hybridized ssDNA was determined by fluorescent resonance energy transfer analysis (FRET, Fig. S6B†). Excess amount of ssDNAa-Cy3 and polymersomes linked with ssDNAa-Cy3 (P20-b-Cy3) were incubated with polymersomes linked with ssDNAb-Cy5 (P20-b-Cy5), respectively. The percentage of hybridized ssDNA, when forming clusters, was calculated by dividing the fluorescence intensity of P20-b-Cy5 hybridized with P20-b-Cy3 by the value when P20-b-Cy5 is hybridized with an excess amount of ssDNAa-Cy3. 50% of non-hybridized ssDNA on the polymersomes' surface is also indicated by the increase in ζ-potential from −11.00 ± 0.04 mV for DY-633-P20-a and −10.60 ± 0.02 mV for ATTO-488-P20-b to −5.47 ± 0.02 mV for the clusters (s.e.m., n = 3, Table S4†). Therefore, the non-hybridized ssDNA on the clusters contributes to their cellular interactions.

2.4. Development of catalytically active DNA-linked polymersome clusters

Capitalizing on the fact that our clusters stably attach to the cell surface, we subsequently focused on developing the clusters for potential detoxification applications in the blood circulation. Polymersome clusters attached to the cell surface of blood vessels and loaded with catalytically active enzymes can be applied as exogenous tool kits that simultaneously protect the encapsulated cargo from degradation or deactivation and can be used for the elimination of circulating toxic chemicals. One solution we envision resides in taking a true and tested enzyme, fungal laccase, and encapsulate it within the polymersomes. Laccases have been extensively used for bioremediation applications, as they are known to act on multiple xenotoxic compounds, such as pesticides and insecticides,[34] anti-inflammatory drugs with a high incidence of misuse and overdose, as for example Acetaminophen and aspirin,[46] phenolic compounds,[47,48] polychlorinated biphenyls (PCBs) and polycyclic aromatic hydrocarbons (PAH).[49] While actions to reduce the exposure to such toxins have been taken, microplastics, ubiquitously present in the environment are now making their way up the food chain and represent a new source of concern as they leach out PCBs, phenolic substances and various other endocrine disrupting compounds.[50] Phenolic substances are main chemical pollutants in soil and water and their production is tremendous: for example, the annual output of biphenyl A alone is up to 4.69 million tons.[51] Luckily laccases can also degrade such substrates relieving the toxic burden.[52]

Here as a proof of concept we encapsulate laccase in polymersomes permeabilized by inserting the outer membrane protein F (OmpF) into the membrane. We confirm that upon encapsulation, either in single, unmodified polymersomes (Lac-Polymersomes) or in DNA-clustered Lac-Polymersomes, laccase maintains its activity and converts the substrate Amplex Ultra Red to the fluorescent product resorufin (Fig. 4). At the same concentration, both unmodified and clustered Lac-Polymersomes show 40% of the activity of free enzymes, whereas almost no activity can be detected from control Lac-Polymersomes with no OmpF because their membrane is not permeable for small molecules. In human serum, the DNA-clustered Lac-Polymersomes truly exhibit their advantages, displaying an increase in activity up to 80% of the activity of free laccase in the same medium (Fig. 4). Previously, we have shown that encapsulation not only helps maintain enzymatic activity in complex medium, but also increases the stability of the enzymes and protects them from degradation.[44] In serum,

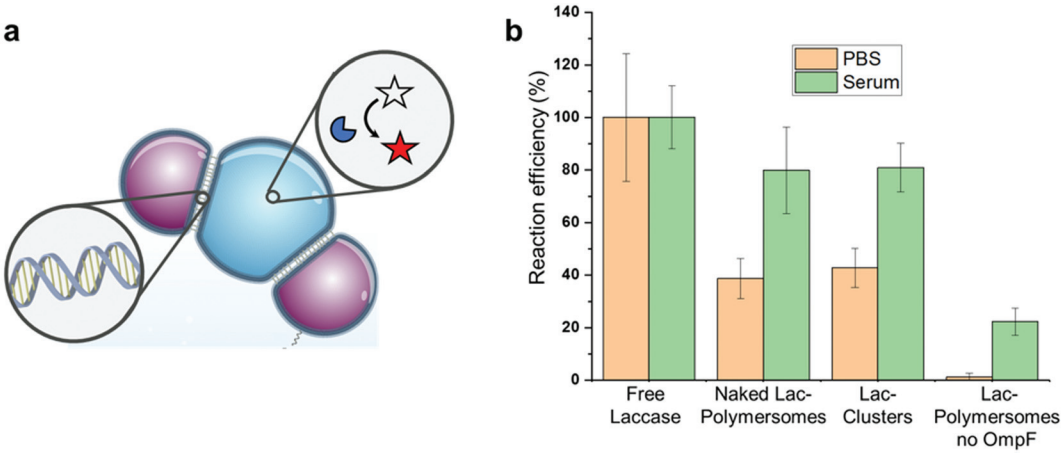

Fig. 4 Catalytic activity of DNA-polymersome clusters containing laccase. (A) Schematic representation of DNA-linked polymersome cluster with catalytic activity by encapsulation of laccase (Lac) and permeabilization of the polymer membrane by insertion of OmpF. The encapsulated enzyme laccase converts *in situ* Amplex Ultra Red to the fluorescent product resorufin. (B) Reaction efficiency of the free laccase, non-ssDNA modified polymersomes containing encapsulated laccase (Naked Lac-Polymersomes), DNA-clustered Lac-Polymersomes equipped with OmpF, and control Lac-Polymersomes that are not permeabilized (without OmpF). Reaction efficiency was determined by measuring the production of resorufin (Ex. λ = 529 nm, Em. λ = 600 nm; n = 3) both in PBS (orange) and in human serum (green).

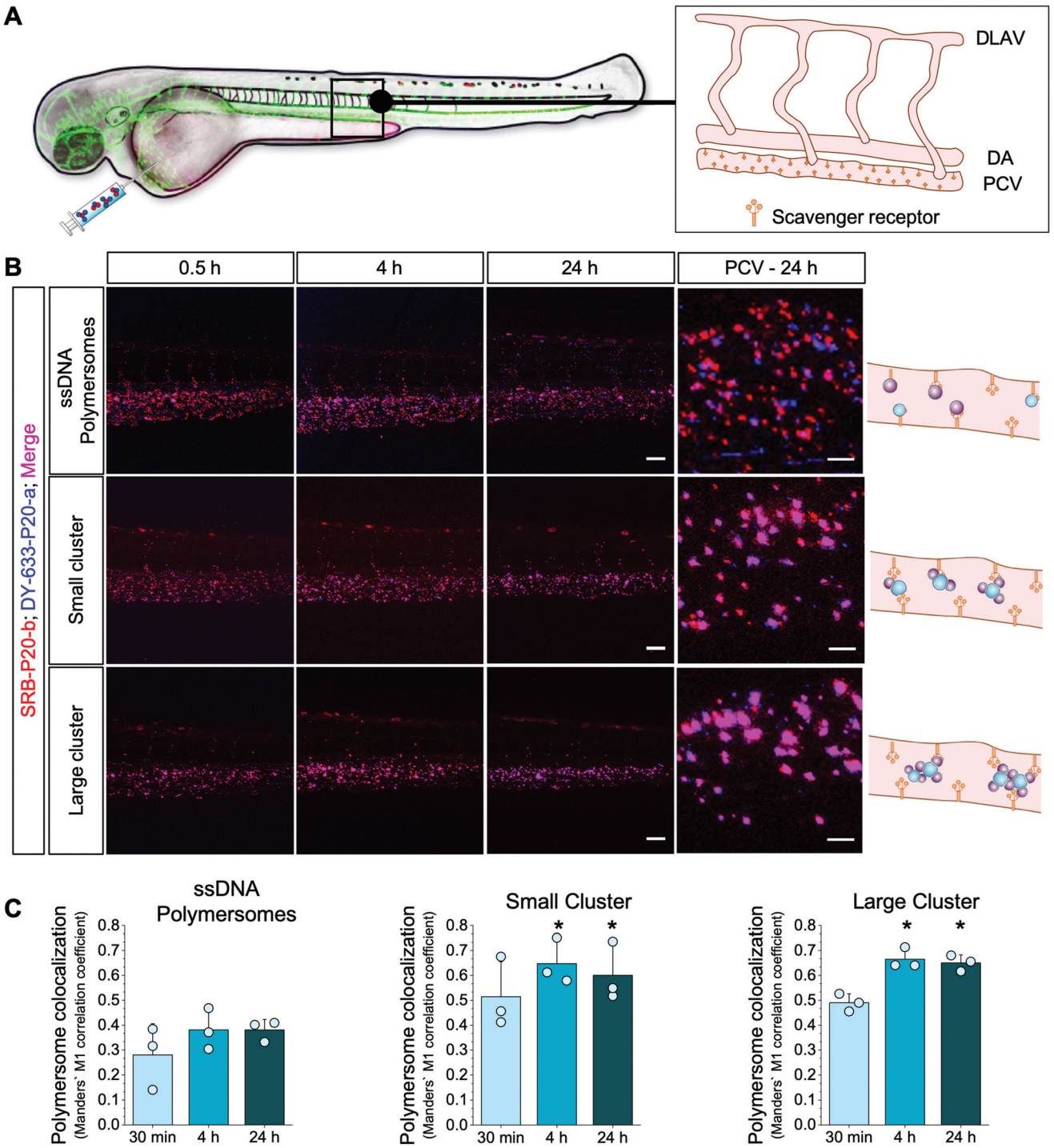

Fig. 5 Biodistribution and stability of DNA-linked polymersome clusters *in vivo*. (A) Schematic representation of anatomical regions in the zebrafish model (DLAV = dorsal longitudinal anastomotic vessel, DA = dorsal aorta, PCV = posterior cardinal vein lined with scavenger receptors). Non-coupling ssDNA polymersomes (SRB-P20-a and Dy-633-P20-a), small clusters and large clusters were injected into transgenic zebrafish embryos. CLSM micrographs from the tail region were taken at specific time points after intravenous injection. Auto-fluorescence of pigment cells (bright red spots) are visible in the dorsal region. (B) Time-dependent analysis of biodistribution of non-coupling ssDNA polymersomes or preformed DNA-linked polymersome clusters (small clusters – 300 nm and big clusters – 500 nm) at 0.5, 4 and 24 hours (left). Scale bars = 50 μm. Schematic presentation and biodistribution analysis of non-coupling polymersomes, small clusters and large clusters in PCV. Representative high magnification images are shown (right). Scale bar = 10 μm. (C) Colocalization analysis of DY-633-P20-a and SRB-P20-b modified polymersomes, small clusters (average size 300 nm) and larger clusters (average size 500 nm) *in vivo* based on Manders' M1 colocalization coefficient. Statistical analysis was performed by one-way ANOVA with a Bonferroni *post hoc* test. * $p < 0.05$ *vs.* non-coupling polymersomes at the same time point (means ± s.e.m., $n = 3$).

free laccases were partially degraded while the ones inside the polymersomes and clusters were protected. However, in serum trace amounts of heme-containing proteins lead to further oxidation of Amplex Ultra Red, causing a higher background than observed in PBS. Nevertheless, by combining the robust DNA-cluster system that attaches to the cell surface with the catalytic capability of these clusters, we can utilize our system as extracellular detoxification patches. In addition, the clusters provide a better spatial localization than single-polymersomes, especially supported by their specific interactions with the cells. With future optimization, our enzyme loaded networks could become a first line of protection for farmers under constant exposure to pesticides and insecticides, for patients with increased levels of xenobiotics in their blood or for those with increased levels of microplastics in their system.

2.5. Examination of DNA-linked polymersome cluster behavior *in vivo*

We finally examined the *in vivo* behavior of ssDNA–polymersome clusters (*i.e.* biodistribution, cluster stability) using the zebrafish as a vertebrate screening model. Recently, it has been shown that the zebrafish model is a straightforward tool to study the systemic circulation and biodistribution of nanoparticles[53] and the stability as well as enzymatic activity of artificial organelles.[25] Therefore, we investigated mixtures of non-complementary ssDNA–polymersomes encapsulating either sulforhodamine B (SRB) or DY-633, as small molecule mimics, and small and large polymersome clusters in transgenic *kdrl:EGFP* zebrafish embryos, which express EGFP in their vasculature endothelial cells. We injected all nanostructures intravenously into the blood circulation *via* the duct of Cuvier (Fig. 5A and Fig. S6F, G† – characterization of clusters with encapsulated SRB and DY-633 used in this *in vivo* study) and analyzed the *in vivo* biodistribution at specific time points (0.5, 4, and 24 h) using CLSM (Fig. 5B). Interestingly, polymersome mixtures as well as both small and large clusters showed a distinct binding pattern in the caudal vein region already after 30 min. After 24 hours all types of polymersomes remained attached to the posterior caudal vein (PCV, Fig. 5B). This is an interesting observation, since this region has been identified as a model to assess the interaction of anionic nanoparticles with scavenger receptors.[54] Thus, both ssDNA–polymersomes and the polymersome clusters were also recognized *in vivo* by scavenger receptor expressing cells, confirming our *in vitro* results.

To assess the *in vivo* stability of non-complementary ssDNA polymersomes, small and large clusters, we performed a colocalization analysis of DY-633-P20-a and SRB-P20-b bearing polymersome signals (Fig. 5C). In the case of non-complementary polymersome mixtures, both polymersome types showed a strong binding to the same scavenger receptor expressing regions, however with very low colocalization at all time points (30 min: 0.28 ± 0.07; 4 h: 0.38 ± 0.05; 24 h: 0.38 ± 0.02, mean ± s.e.m., n = 3). Thus, non-complementary polymersomes do not assemble into clusters in blood circulation but bind to the same target region. In sharp contrast, preformed polymersome clusters exhibited a significantly higher colocalization of DY-633-P20-a and SRB-P20-b signals at binding sites *in vivo* (Fig. 5B and C). Manders' M1 colocalization coefficients 24 h post injection were 0.60 ± 0.07 and 0.65 ± 0.02 (mean ± s.e.m., n = 3) for small and large polymersome clusters, respectively. Thus, the multiple factors that influence the disassembly of DNA-linked nanomaterials such as serum proteins, enzymes or shear force did not affect the polymersome clusters' integrity over time, confirming their stability even under *in vivo* conditions.

3. Conclusions

In summary, we have developed soft DNA-linked assemblies based on hierarchical organization of polymersomes that show specific interactions with cell surfaces with exceptional stability *in vitro* and *in vivo* thus strengthening our vision of developing them for biological applications. We demonstrated the ability to control the size of DNA-linked polymersome clusters by varying the ssDNA surface density. *In vitro* and *in vivo* behavior of the clusters are a direct result of the inherent deformability and membrane fluidity of the polymersomes, where a fraction of the ssDNAs can migrate to the protective bridging regions, while the remaining unbound ssDNA fraction can interact with scavenger receptors on the surface of epithelial cells. Finally, we also demonstrated that a medically relevant enzyme can be encapsulated within the DNA-polymersome clusters and maintains its activity. Polymersome clusters have the following advantages as compared to non-clustered or ss-DNA-polymersomes: (i) they allow segregated nano-spaces where different reactions can take place simultaneously, (ii) support co-localization of polymersomes inducing an increase in their overall functionality, (iii) tend to have better binding to the cell surface and (iv) accumulate more on the cell surface, thus supporting an improved functionality. In addition, polymersome clusters are physiochemically stable in the physiological environment and strongly attach to scavenger receptor-expressing cells thus making them ideal candidates to serve as nano-implants for sustainable and long-term therapies. The unique *in vitro* and *in vivo* properties and robustness propel this system towards the development of protective detoxification networks. More importantly, the global enzyme replacement treatment market is expected to grow 6.5% per year and generate more than $13.7 billion each year by 2028.[55] Our new approach and results could be extended to the enzyme replacement market by replacing the encapsulated enzyme to protect and deliver a broad context of therapeutic enzymes to selective cells and complement cell functions in blood circuits.

4. Materials and methods

See the ESI† for additional details. As a reporting standard has been developed to strengthen the quality and reproducibility

of published research in the field of bio-nano science,[56] we provide information of materials including synthesis and characterization, size distribution, shape, dimensions, aggregation, zeta potentials, density (in culture), enzyme loading efficiency, labelling efficiency, stability in biological fluids, as well as biological characterization including toxicity, 3D-mapping of materials on cell surfaces for selective targeting quantification, mechanism of selective targeting, material distribution in Zebra fish, and statistics for data analysis.

4.1. Materials

Hydroxylethoxypropyl terminated polydimethylsiloxane was purchased from ABCR GmbH (AB 116675), Germany. The oligonucleotides with DBCO modification on the 5′-end and the ones with both DBCO modification on the 5′-end and ATTO 488/Cy5 modification on the 3′-end were purchased from IBA GmbH, Germany. DBCO-OEG_4-ATTO 488 was purchased from Jena Bioscience, Germany. The fluorescent probes ATTO 488 and DY-633 were purchased from ATTO-TEC GmbH, Germany, and Dyomics GmbH, Germany, respectively. $CHCl_3$ in HPLC-grade quality for GPC elution were obtained from Scharlab, Spain. All other chemicals were purchased from Sigma-Aldrich in the highest available grade and used as received if not stated otherwise.

4.2. Block copolymers

$PDMS_{62}$-$PMOXA_{13}$ was synthesized according to the published procedure.[57] $PDMS_{62}$-$PMOXA_{13}$-OH: ^{1}H NMR (400 MHz, δ, $CDCl_3$): 0 ppm (m, –Si(CH_3)$_2$), 0.54 ppm (m, –SiCH_2), 0.88 ppm (t, –CH_3), 1.31 ppm (m, –CH_2–CH_2–), 1.62 ppm (m, –SiCH_2–CH_2–CH_2O–), 2.08–2.21 ppm (m, CH_3–C═O), 3.40–3.60 ppm (m, –CH_2–O–CH_2–CH_2–N–CH_2–CH_2–), 3.75 ppm (t, –CH_2OH).

For the synthesis of N_3-functionalized polymer, $PDMS_{65}$-$PMOXA_{32}$ (400 mg, 54.0 μmol) was dissolved in 5 mL anhydrous $CHCl_3$, following the addition of 14-azido-3,6,9,12-tetraoxatetradecanoic acid solution (0.5 M in *tert*-butyl methyl ether, 2.6 eq.), *N*,*N*′-dicyclohexylcarbodiimide (DCC, 2.6 eq.), triethylamine (5.2 eq.) and 4-dimethylaminopyridine (0.2 eq.) under Ar flow. The reaction flask was placed in an ice bath at 0 °C, warmed to room temperature gradually and reacted further for 2 days. The crude azide-functionalized diblock copolymers were purified by dialysis (MWCO 3.5 kDa) in H_2O/EtOH (4 : 6 V/V). ^{1}H NMR (400 MHz, $CDCl_3$): 0 ppm (m, –Si(CH_3)$_2$), 0.54 ppm (m, –SiCH_2), 0.88 ppm (t, –CH_3), 1.31 ppm (m, –CH_2–CH_2–), 1.62 ppm (m, –SiCH_2–CH_2–CH_2O–), 2.08–2.21 ppm (m, CH_3–C═O), 3.40–3.60 ppm (m, –CH_2–O–CH_2–CH_2–N–CH_2–), 3.65 ppm (s, –O–CH_2–CH_2–O–CH_2–CH_2–O–CH_2–CH_2–O–CH_2–).

4.3. ssDNA–polymersomes

Polymersome formation. The block copolymers, $PDMS_{62}$-$PMOXA_{13}$ and $PDMS_{71}$-$PMOXA_{25}$-OEG_3-N_3, were dissolved in ethanol and chloroform, respectively, to yield stock solutions with a concentration of 10 mg mL^{-1} and mixed in the respective ratio to prepare polymersomes with various amounts of azide groups on the polymersome' surface. $PDMS_{62}$-$PMOXA_{13}$ (400 μL × 10 mg mL^{-1}, 4 mg, 5800 g mol^{-1} measured by GPC, 0.7 μmol) was mixed with 0.5 (2.3 μL × 10 mg mL^{-1}, 0.023 mg, 6400 g mol^{-1} measured by GPC, 3.6 nmol), 1, 5, 10, 20 and 33 mol% of $PDMS_{71}$-$PMOXA_{25}$-OEG_3-N_3 in a 5 mL round-bottom flask, followed by solvent removal on a rotary evaporator (140 mbar, 40 °C, 75 rpm). The thin polymer film was rehydrated by adding 1 mL PBS and stirred overnight at room temperature. The yielded solution was extruded with an Avanti mini-extruder (Avanti Polar Lipids, Alabama, USA) through a polycarbonate (PC) membrane with a 200 nm diameter pore size for 15 times to unify the size of polymersomes.

To visualize the polymersomes by CLSM, 0.2 mM ATTO 488, 0.2 mM DY-633 or 0.2 mM SRB was dissolved in 1 mL PBS and used for the film rehydration instead of PBS to prepare the polymersomes P20. Dye-encapsulated polymersomes were extruded as mentioned above and purified from non-encapsulated fluorescent probes by size exclusion chromatography (SEC, Sepharose 4B column; 8 cm length). The fraction of individual non-encapsulated fluorescent probes was collected and the concentration was determined by measuring the maximal UV-vis absorbance. The maximal molar extinction coefficient (ε_{max}) of ATTO 488 (λ_{max} = 500 nm) DY-633 (λ_{max} = 637 nm) and SRB (λ_{max} = 550 nm) is 9 × 10^4, 17 × 10^4 and 11 × 10^4 M^{-1} cm^{-1}, respectively. The encapsulation efficiency of ATTO 488, DY-633 and SRB for P20 is subsequently calculated as 10.4%, 24.7% and 18.7%, respectively (eqn (1)).

$$E = \frac{N_0 - N_f}{N_0} \quad (1)$$

E is the encapsulation efficiency, N_0 is the initial moles of the dye used for encapsulation and N_f is the moles of the free dye after encapsulation.

Coupling of DBCO-OEG_4-ATTO 488 to polymersomes. 100 μL of 4 mg mL^{-1} of polymersomes with different N_3 content were incubated with DBCO-OEG_4-ATTO 488 (1.2 eq. per azide group) in Eppendorf tubes (capacity 200 μL), at 37 °C and 300 rpm for 24 h. The unreacted DBCO-OEG_4-ATTO 488 was removed by SEC eluted by PBS (Sepharose 4B column; 8 cm length). The volume of samples after purification was measured and the concentration of purified DBCO-ATTO 488-labled polymersomes (weight of polymer in solution) was calculated.

Conjugation of ssDNA to polymersomes. 100 μL of 4 mg mL^{-1} of polymersomes with different N_3 content were incubated with various amounts of 22 bp DBCO-ssDNAa or the complementary DBCO-ssDNAb (1 eq. per azide group), at 37 °C 300 rpm for 2.5 days. The total volume of sample solution used is always more than 100 μL to avoid drying the polymersomes due to water evaporation. The ssDNA–polymersomes were purified by SEC and the concentration was calculated as mentioned above. ssDNAa-488 and ssDNAb-Cy5 were conjugated to distinct polymersomes by the same procedure for the quantification of ssDNAa and ssDNAb per polymersome. Additionally, the conjugation of ssDNA to dye-encapsulated polymersomes was performed by the same procedure for the visualization *in vitro* and *in vivo*. Non-encapsulated free dyes and non-linked free ssDNA was removed together by SEC. To

prepare large clusters for *in vitro* and *in vivo* studies, the conjugation of ssDNA to dye-encapsulated P20 was slightly modified. The concentration of polymersomes and the corresponding ssDNAa/b was doubled to increase the reaction efficiency, thereby resulting higher number of ssDNA per polymersomes.

4.4. DNA-linked polymersome clusters

Formation of polymersome clusters. In general, the polymersome clusters were prepared by incubating 0.1 mg mL^{-1} of ssDNAa-polymersomes with 0.1 mg mL^{-1} of the corresponding ssDNAb-polymersomes at 37 °C. Dye-encapsulated polymersomes were used for *in vitro* and *in vivo* studies. The apparent D_H of clusters was monitored by DLS as a function of time and all of them except that of P33-ab reached to a plateau after 24 h incubation at 37 °C. Therefore, the preparation of all polymersome clusters except large clusters for *in vitro* and *in vivo* studies were performed at 37 °C at least for one day to assure that no further increase of the apparent D_H would occur. P-a and the corresponding P-b were prepared from the same parent polymersomes bearing azide groups to minimize the deviation of polymersomes' concentration from different batches. Additionally, as polymersomes bearing larger amount of ssDNA assembled rapidly, they were incubated at RT for 6 h and kept in the fridge before the utilization for *in vitro* and *in vivo* study.

DNase I digestion. 0.2 mg mL^{-1} of P1-ab, P5-ab, P10-ab and P20-ab polymersome clusters were diluted in PBS to reach a concentration of 0.025 mg mL^{-1}, 0.05 mg mL^{-1} and 0.1 mg mL^{-1}. The diluted polymersome cluster solutions were further treated with various concentrations of DNase I (0.1 μg mL^{-1}, 1 μg mL^{-1} and 10 μg mL^{-1}, final volume 400 μL) in presence of 5 mM of the cofactor $MgCl_2$. All samples were incubated at 37 °C for 1 day followed by DLS measurements for the size analysis. For the control experiment, 0.1 mg mL^{-1} of P20-a and P20-b were pre-treated with 1 μg mL^{-1} of DNase I at 37 °C for 24 h, respectively, and mixed at 37 °C for another 24 h, following up with characterization of TEM. In order to understand the influence of DNA length on the nuclease resistance of polymersome clusters, polymersomes were linked with complementary 11 bp ssDNA, respectively, and purified as aforementioned. The sequences of 11 bp ssDNA are 5′-DBCO-CCT CGC TCT GC-ATTO 488-3′ and 5′-DBCO-GCA GAG CGA GG-ATTO 643N-3′, respectively. The DNA density on the polymersome' membrane was carefully controlled in order to obtain the polymersome clusters with a size similar to P20-ab. 0.025 mg mL^{-1}, 0.05 mg mL^{-1} and 0.1 mg mL^{-1} of polymersome clusters linked by 11 bp DNAs was treated with DNase I at 0.1 μg mL^{-1}, 1 μg mL^{-1} and 10 μg mL^{-1} at 37 °C for 1 day, respectively. The samples were incubated followed by characterization as aforementioned for polymersome clusters.

Stability of polymersome clusters in cell medium with serum. 0.025 mg mL^{-1} of P20-ab polymersome clusters were incubated in cell medium with serum. The change of the size at 37 °C was continually recorded by DLS.

FRET analysis. P20 was conjugated with ssDNAa-Cy3 or ssDNAb-Cy5, purified as mentioned above, and used for the FRET analysis. Firstly, 400 μL of 0.2 mg mL^{-1} of P20-b-Cy5 was added with excess amount of ssDNAa-Cy3 and the increase in florescence emission at 660 nm (λ_{ex} = 530 nm) caused by the hybridization of free ssDNAa-Cy3 to ssDNAb-Cy5 on the polymersome's surface due to FRET was recorded by fluorimeter. Secondly, 200 μL of 0.4 mg mL^{-1} of P20-b-Cy5 was added with 200 μL of 0.4 mg mL^{-1} of P20-a-Cy3. The increase in florescence emission at 660 nm was recorded as aforementioned. The fluorescence intensity of ssDNAa-Cy3 and P20-a-Cy3 as a function of time at 660 nm was recorded additionally and subtracted from data to avoid any contribution to fluorescence intensity when calculating FRET efficiency. The percentage of hybridized ssDNA when forming clusters was calculated by dividing the increase of fluorescence intensity of P20-b-Cy5 hybridizing with P20-a-Cy3 with the value when P20-b-Cy5 hybridized with excess amount of ssDNAa-Cy3. The size change when P20-b-Cy5 mixing with P20-a-Cy3 was monitored by DLS, which proved the cluster formation during the FRET analysis.

4.5. *In vitro* studies of the behavior of the DNA-linked polymersome clusters

Cell culture. HEK293T (embryonic kidney, human; ATCC, CRL-3216), HeLa (epitheloid cervix carcinoma, human; ATCC, CCL-2) and U87-MG (glioblastoma cells obtained from the University of Basel Hospital) were cultured in Dulbecco's Modified Eagle Medium (DMEM, Gibco Life Sciences) with GlutaMAX™-I and supplemented with 10% FCS (BioConcept), 100 units per mL penicillin and 100 μg mL^{-1} streptomycin (Sigma Aldrich). Cells were maintained at 37 °C and 5% CO_2.

Cell viability assay. CellTiter 96® AQueous One Solution Cell Proliferation Assay (MTS, Invitrogen) was used in accordance with the provided protocol to determine cell viability. HeLa cells were seeded in a 96 well plate (3000 cells per well) and cultured for 24 h at 37 °C and 5% CO_2. After 24 h 40 μL of 0.2 mg mL^{-1} unfunctionalized polymersomes, polymersomes containing 20% azide, ssDNA-a polymersomes, ssDNA-b polymersomes, or polymersome clusters were added to the cells to reach a final volume of 200 μL and incubated further for 24 h. The MTS reagent (20 μL) was added to each well and absorbance at 490 nm was measured after 2 h using a Spectramax plate reader. Background absorbance was subtracted from each well and data was normalized to control cells. Experiments were done in quadruplicate (n = 4) and data was plotted using GraphPad Prism.

Cell imaging experiments. HEK293T, HeLa and U87 MG cells were seeded (3×10^4 cells in 300 μL cell culture medium per well) in 8-well ibidi collagen IV coated plates. After 24 h the cell culture medium was removed and replaced with 280 μL fresh culture medium (DMEM-GlutaMAX™-I with 10% FCS, 1% penicillin/streptomycin). Next, we added unmodified polymersomes, ssDNAa polymersomes (DY-633-P20a) or polymersome clusters to the cells (20 μL, 0.2 mg mL^{-1}) and incubated further for 24 h. Before live cell imaging, we washed the cells 4× with Opti-MEM (Gibco Life Sciences) and stained the cell membrane with CellMask™ orange plasma stain accord-

ing to provided protocol (Invitrogen). After staining, cells were further washed 3× and imaged by CLSM.

Flow cytometry. HEK293T, HeLa and U87 MG cells were seeded (1.2×10^5 cells per well, 360 μL final volume) in 24-well plates in cell culture medium. After 24 h, 40 μL of 0.2 mg mL^{-1} unfunctionalized polymersomes, ssDNA-a polymersomes, small clusters or large clusters were added to the cells and further incubated for 24 h. Cells were then washed with PBS and trypsinized with 150 μL trypsin-EDTA (Sigma Aldrich). Cells were resuspended in cell media, transferred to 1.5 mL microcentrifuge tubes and centrifuged for 5 min at 1 rcf. The supernatant was removed and the cell pellet resuspended in 500 μL cold PBS and put on ice until flow cytometry analysis. Flow cytometry analysis was performed using a BD FACSCanto II flow cytometer (BD Bioscience, USA). Doublets were excluded using FSC and SSC detectors, single cells were excited at 488 nm or 633 nm and the emission was detected in FL1 (530/30; Atto488 Channel) and FL3 (630/30 DY-633 Channel). A total of 10 000 single cells for each sample were analyzed, and data processed using Flow Jo VX software (TreeStar, Ashland, OR).

Inhibition of cluster binding. HEK293T cells were seeded in 8-well collagen IV coated plates (ibidi) as described above. Cells were then treated with either polyinosinic acid or Fucoidan (10 μg ml^{-1} or 50 μg mL^{-1} final concentrations). After 1 h, ssDNA–polymersomes, small or large clusters (20 μL, 0.2 mg mL^{-1}) were added to the cells and incubated further for 24 h. Cells were then washed, stained and imaged using the same procedure as described above to allow for comparison.

Formation of DNA-polymersome clusters with encapsulated laccase. $PDMS_{62}$-$PMOXA_{13}$ (400 μL × 10 mg mL^{-1}) was mixed with 20 mol% of $PDMS_{71}$-$PMOXA_{25}$-OEG_3-N_3 in a 5 mL round-bottom flask, followed by solvent removal. The polymer film was rehydrated by adding 950 μL PBS containing 1 mg mL^{-1} of laccase from *t. versicolor* (EC 1.10.3.2) and 50 μL of previously expressed, purified and dialyzed OmpF (60 μg mL^{-1} final concentration), as previously described[44] and stirred overnight at room temperature. As a control, polymersomes with laccase and no OmpF were prepared. The resulting polymersomes were then extruded through a 200 nm diameter pore membrane size 15 times as described above. Free laccase was removed using a Sepharose 4B size exclusion column (30 cm length). The non-encapsulated laccase fraction was recovered from the control polymersomes with no OmpF during purification by size exclusion chromatography and its concentration quantified at 280 nm with Nanodrop 2000 (Thermo Fisher Scientific, USA), using the MW and ε calculated from the amino acid sequence on ExPASy. By subtracting the total amount present in the non-encapsulated fraction from the added amount of laccase, the final enzyme concentration in the sample was calculated to be 421 μg mL^{-1} for naked polymersomes and 0.42 μg mL^{-1} after ssDNA conjugation.

Enzymatic activity assay. The enzymatic assays were performed by following the production of resorufin (Ex. λ = 529 Em. λ = 600 nm) from Amplex Ultra Red thanks to the action of the laccase catalytic polymersomes (Lac-Polymersomes).[58] Briefly, in a black flat-bottomed 96-well plate (Thermo Fisher Scientific, USA), either free laccase, naked Lac-Polymersomes or DNA-lined Lac-Polymersome clusters were added to a final concentration of 6 μg mL^{-1}, with AR (final concentration 1 μM) in either PBS or male human serum to a final volume of 0.2 mL. The fluorescence was measured after 5 minutes, the baseline due to AR autoxidation was subtracted and the reaction efficiency was expressed as $\frac{\text{Intensity}_{\text{Sample}}}{\text{Intensity}_{\text{Free enzyme}}}\%$ with intensity measured as arbitrary fluorescent units.

4.6. *In vivo* studies of the behavior of the DNA-linked polymersome clusters

Zebrafish injection. Zebrafish husbandry and embryo maintenance were performed at standard conditions and in accordance with Swiss animal welfare regulations. Eggs were collected and kept in zebrafish culture media containing 1-phenyl 2-thiourea (PTU) in order to suppress pigment cell formation as already described elsewhere.[59] Small clusters formed by DY-633-P20-a and SRB-P20-b, large clusters formed by DY-633-P20-a and SRB-P20-b, and non-clustered sample containing DY-633-P20-b and SRB-P20-b were injected into zebrafish blood circulation (3 nL, 0.2 mg mL^{-1}) *via* the Duct of Cuvier at 2 days post fertilization (dpf).[60] Injected live zebrafish embryos were casted into 0.3% agarose (w/v) containing 0.01% tricaine (w/v) as anesthetic. Injections were performed using a micromanipulator (Wagner Instrumentenbau DG, Schöffengrund, Germany), a Pico Pump PV830 (WPI, Sarasota, Florida), and a Leica S8APO microscope (Leica, Wetzlar, Germany). Confocal micrographs were taken using an Olympus FV-1000 inverted confocal laser scanning microscope equipped with a 10× UPlanSApo (NA 0.4) and 20× UPlanSApo (NA 0.75) objective. Colocalization analysis based on Manders' M1 colocalization coefficient was performed using the Fiji ImageJ JaCoP plugin.

Author contributions

The manuscript was written through contributions of all authors. All authors have given approval to the final version of the manuscript.

Funding sources

We gratefully acknowledge the financial support provided by the Swiss National Science Foundation (SNSF), the National Centre of Competence in Research Molecular Systems Engineering and the University of Basel. DW is supported by an SNSF Early Postdoc Mobility Fellowship (#174975).

Conflicts of interest

There are no conflicts to declare.

Acknowledgements

Authors thank Prof. W. Meier (University of Basel) for useful discussions regarding the polymer synthesis and Prof. Dr M. Affolter (University of Basel) for supporting zebrafish breeding. CP thanks Dr H. Palivan for statistics analysis and discussions on the relevance of fitting models. R. M. Subasic and D. Hughes are acknowledged for useful discussions and reading the manuscript.

References

1 F. A. Aldaye, A. L. Palmer and H. F. Sleiman, *Science*, 2008, **321**, 1795–1799.
2 R. Merindol, S. Loescher, A. Samanta and A. Walther, *Nat. Nanotechnol.*, 2018, **13**, 730–738.
3 N. Liu and T. Liedl, *Chem. Rev.*, 2018, **118**, 3032–3053.
4 B. Roark, J. A. Tan, A. Ivanina, M. Chandler, J. Castaneda, H. S. Kim, S. Jawahar, M. Viard, S. Talic, K. L. Wustholz, Y. G. Yingling, M. Jones and K. A. Afonin, *ACS Sens.*, 2016, **1**, 1295–1300.
5 V. Raeesi, L. Y. T. Chou and W. C. W. Chan, *Adv. Mater.*, 2016, **28**, 8511–8518.
6 N. L. Rosi, D. A. Giljohann, C. S. Thaxton, A. K. R. Lytton-Jean, M. S. Han and C. A. Mirkin, *Science*, 2006, **312**, 1027–1030.
7 R. Schreiber, J. Do, E.-M. Roller, T. Zhang, V. J. Schüller, P. C. Nickels, J. Feldmann and T. Liedl, *Nat. Nanotechnol.*, 2014, **9**, 74–78.
8 F. Hong, F. Zhang, Y. Liu and H. Yan, *Chem. Rev.*, 2017, **117**, 12584–12640.
9 M. G. Warner and J. E. Hutchison, *Nat. Mater.*, 2003, **2**, 272–277.
10 L. Y. T. Chou, K. Zagorovsky and W. C. W. Chan, *Nat. Nanotechnol.*, 2014, **9**, 148–155.
11 R. C. Mucic, J. J. Storhoff, C. A. Mirkin and R. L. Letsinger, *J. Am. Chem. Soc.*, 1998, **120**, 12674–12675.
12 J. Liu, V. Postupalenko, S. Lörcher, D. Wu, M. Chami, W. Meier and C. G. Palivan, *Nano Lett.*, 2016, **16**, 7128–7136.
13 U. Jakobsen, A. C. Simonsen and S. Vogel, *J. Am. Chem. Soc.*, 2008, **130**, 10462–10463.
14 A. Czogalla, H. G. Franquelim and P. Schwille, *Biophys. J.*, 2016, **110**, 1698–1707.
15 P. A. Beales and T. K. Vanderlick, *J. Phys. Chem. A*, 2007, **111**, 12372–12380.
16 N. Dave and J. Liu, *ACS Nano*, 2011, **5**, 1304–1312.
17 B. S. Pattni, V. V. Chupin and V. P. Torchilin, *Chem. Rev.*, 2015, **115**, 10938–10966.
18 F. Meng, Z. Zhong and J. Feijen, *Biomacromolecules*, 2009, **10**, 197–209.
19 M. Rasoulianboroujeni, G. Kupgan, F. Moghadam, M. Tahriri, A. Boughdachi, P. Khoshkenar, J. J. Ambrose, N. Kiaie, D. Vashaee, J. D. Ramsey and L. Tayebi, *Mater. Sci. Eng., C*, 2017, **75**, 191–197.
20 Y. Xia, J. Tian and X. Chen, *Biomaterials*, 2016, **79**, 56–68.
21 F. Wang, J. Gao, J. Xiao and J. Du, *Nano Lett.*, 2018, **18**, 5562–5568.
22 A. Wijaya and K. Hamad-Schifferli, *Langmuir*, 2007, **23**, 9546–9550.
23 M. Spulber, P. Baumann, J. Liu and C. G. Palivan, *Nanoscale*, 2015, **7**, 1411–1423.
24 C. G. Palivan, R. Goers, A. Najer, X. Zhang, A. Car and W. Meier, *Chem. Soc. Rev.*, 2016, **45**, 377–411.
25 T. Einfalt, D. Witzigmann, C. Edlinger, S. Sieber, R. Goers, A. Najer, M. Spulber, O. Onaca-Fischer, J. Huwyler and C. G. Palivan, *Nat. Commun.*, 2018, **9**, 1127–1138.
26 H. Che and J. C. M. van Hest, *J. Mater. Chem. B*, 2016, **4**, 4632–4647.
27 G.-Y. Liu, C.-J. Chen and J. Ji, *Soft Matter*, 2012, **8**, 8811–8821.
28 J. Gaitzsch, X. Huang and B. Voit, *Chem. Rev.*, 2016, **116**, 1053–1093.
29 S. Ohta, D. Glancy and W. C. W. Chan, *Science*, 2016, **351**, 841–845.
30 J. Kim, Y. M. Lee, Y. Kang and W. J. Kim, *ACS Nano*, 2014, **8**, 9358–9367.
31 H. Li, X. Zhou, D. Yao and H. Liang, *Chem. Commun.*, 2018, **54**, 3520–3523.
32 M. T. Stephan, J. J. Moon, S. H. Um, A. Bershteyn and D. J. Irvine, *Nat. Med.*, 2010, **16**, 1035–1041.
33 C. M. Csizmar, J. R. Petersburg and C. R. Wagner, *Cell Chem. Biol.*, 2018, **25**, 931–940.
34 D. M. Mate and M. Alcalde, *Microb. Biotechnol.*, 2017, **10**, 1457–1467.
35 A. D. Moreno, D. Ibarra, M. E. Eugenio and E. Tomás-Pejó, *J. Chem. Technol. Biotechnol.*, 2020, **95**, 481–494.
36 K. Kiene, S. H. Schenk, F. Porta, A. Ernst, D. Witzigmann, P. Grossen and J. Huwyler, *Eur. J. Pharm. Biopharm.*, 2017, **119**, 322–332.
37 A. Najer, D. Wu, A. Bieri, F. Brand, C. G. Palivan, H.-P. Beck and W. Meier, *ACS Nano*, 2014, **8**, 12560–12571.
38 Q. Luo, Z. Shi, Y. Zhang, X.-J. Chen, S.-Y. Han, T. Baumgart, D. M. Chenoweth and S.-J. Park, *J. Am. Chem. Soc.*, 2016, **138**, 10157–10162.
39 C. H. J. Choi, L. Hao, S. P. Narayan, E. Auyeung and C. A. Mirkin, *Proc. Natl. Acad. Sci. U. S. A.*, 2013, **110**, 7625–7630.
40 X. Yi and H. Gao, *Soft Matter*, 2015, **11**, 1107–1115.
41 X. Yi, X. Shi and H. Gao, *Phys. Rev. Lett.*, 2011, **107**, 098101–098105.
42 J. Yue, T. J. Feliciano, W. Li, A. Lee and T. W. Odom, *Bioconjugate Chem.*, 2017, **28**, 1791–1800.
43 J. Yan, C. Hu, P. Wang, B. Zhao, X. Ouyang, J. Zhou, R. Liu, D. He, C. Fan and S. Song, *Angew. Chem., Int. Ed.*, 2015, **54**, 2431–2435.
44 A. Belluati, I. Craciun, J. Liu and C. G. Palivan, *Biomacromolecules*, 2018, **19**, 4023–4033.
45 P. C. Patel, D. A. Giljohann, W. L. Daniel, D. Zheng, A. E. Prigodich and C. A. Mirkin, *Bioconjugate Chem.*, 2010, **21**, 2250–2256.

46 J. Yang, W. Li, T. B. Ng, X. Deng, J. Lin and X. Ye, *Front. Microbiol.*, 2017, **8**, 832–856.
47 Z. Asadgol, H. Forootanfar, S. Rezaei, A. H. Mahvi and M. A. Faramarzi, *J. Environ. Health Sci. Eng.*, 2014, **12**, 93.
48 J. M. Bollag, K. L. Shuttleworth and D. H. Anderson, *Appl. Environ. Microbiol.*, 1988, **54**, 3086–3091.
49 Shraddha, R. Shekher, S. Sehgal, M. Kamthania and A. Kumar, *Enzyme Res.*, 2011, **2011**, 217861.
50 M. Smith, D. C. Love, C. M. Rochman and R. A. Neff, *Curr. Environ. Health Rep.*, 2018, **5**, 375–386.
51 L. Zhao, Q. Wu and A. Ma, *IOP Conf. Ser. Earth Environ. Sci.*, 2018, **111**, 012024.
52 G. Macellaro, C. Pezzella, P. Cicatiello, G. Sannia and A. Piscitelli, *BioMed Res. Int.*, 2014, **2014**, 614038.
53 S. Sieber, P. Grossen, P. Detampel, S. Siegfried, D. Witzigmann and J. Huwyler, *J. Controlled Release*, 2017, **264**, 180–191.
54 F. Campbell, F. L. Bos, S. Sieber, G. Arias-Alpizar, B. E. Koch, J. Huwyler, A. Kros and J. Bussmann, *ACS Nano*, 2018, **12**, 2138–2150.
55 H. Tiwari and P. Mhaisekar, Enzyme Replacement Therapy Market - Global Industry Analysis, Size and Forecast, 2018 to 2028, https://www.futuremarketinsights.com/reports/enzyme-replacement-therapy-market, (accessed July 16, 2019).
56 M. Faria, M. Björnmalm, K. J. Thurecht, S. J. Kent, R. G. Parton, M. Kavallaris, A. P. R. Johnston, J. J. Gooding, S. R. Corrie, B. J. Boyd, P. Thordarson, A. K. Whittaker, M. M. Stevens, C. A. Prestidge, C. J. H. Porter, W. J. Parak, T. P. Davis, E. J. Crampin and F. Caruso, *Nat. Nanotechnol.*, 2018, **13**, 777.
57 D. Wu, M. Spulber, F. Itel, M. Chami, T. Pfohl, C. G. Palivan and W. Meier, *Macromolecules*, 2014, **47**, 5060–5069.
58 T. Wang, Y. Xiang, X. Liu, W. Chen and Y. Hu, *Talanta*, 2017, **162**, 143–150.
59 S. Sieber, S. Siegrist, S. Schwarz, F. Porta, S. H. Schenk and J. Huwyler, *Macromol. Biosci.*, 2017, **17**, 1700015–1700024.
60 B. M. Weinstein, D. L. Stemple, W. Driever and M. C. Fishman, *Nat. Med.*, 1995, **1**, 1143–1147.